Structure of the metal-independent restriction enzyme BfiI reveals fusion of a specific DNA-binding domain with a nonspecific nuclease

Saulius Grazulis*†, Elena Manakova*, Manfred Roessle‡, Matthias Bochtler§¶, Giedre Tamulaitiene*, Robert Huber†‖, and Virginijus Siksnys*†

*Laboratory of Protein–DNA Interaction, Institute of Biotechnology, Graiciuno 8, LT-02241 Vilnius, Lithuania; ‡European Synchrotron Radiation Facility, B.P. 220, F-38043 Grenoble Cedex, France; §Department of Structural Biology, International Institute of Molecular and Cell Biology, Księcia J. Trojdena Street 4, 02-109 Warsaw, Poland; ¶Max-Planck-Institut für Molekulare Zellbiologie und Genetik, Pfotenhauerstrasse 108, 01307 Dresden, Germany; and ‖Abteilung Strukturforschung, Max-Planck-Institut für Biochemie, Am Klopferspitz 18a, D-82152 Martinsried, Germany

Contributed by Robert Huber, September 20, 2005

Among all restriction endonucleases known to date, BfiI is unique in cleaving DNA in the absence of metal ions. BfiI represents a different evolutionary lineage of restriction enzymes, as shown by its crystal structure at 1.9-Å resolution. The protein consists of two structural domains. The N-terminal catalytic domain is similar to Nuc, an EDTA-resistant nuclease from the phospholipase D superfamily. The C-terminal DNA-binding domain of BfiI exhibits a β-barrel-like structure very similar to the effector DNA-binding domain of the Mg^{2+}-dependent restriction enzyme EcoRII and to the B3-like DNA-binding domain of plant transcription factors. BfiI presumably evolved through domain fusion of a DNA-recognition element to a nonspecific nuclease akin to Nuc and elaborated a mechanism to limit DNA cleavage to a single double-strand break near the specific recognition sequence. The crystal structure suggests that the interdomain linker may act as an autoinhibitor controlling BfiI catalytic activity in the absence of a specific DNA sequence. A PSI-BLAST search identified a BfiI homologue in a *Mesorhizobium* sp. BNC1 bacteria strain, a plant symbiont isolated from an EDTA-rich environment.

restriction endonuclease | x-ray crystallography

Restriction endonucleases (REases) protect bacteria by hydrolyzing invading viral or other foreign DNA. Type II REases perform their function by catalyzing the sequence-specific cleavage of double-stranded DNA molecules in the presence of Mg^{2+} ions within or close to their recognition sites (1). Surprisingly, orthodox REases and bacteriophage λ-exonuclease that binds a free end of double-stranded DNA and processively degrades one strand in the 5′ to 3′ direction share a similar catalytic mechanism and a common structural ancestor (2). A λ-exonuclease-like domain has been identified in many Mg^{2+}-dependent nucleases involved in DNA recombination and repair (3–5), suggesting that it has been remolded during evolution to perform different functions. To constrain cleavage at specific sites, REases had to develop effective means to control nucleolytic activity of λ-exonuclease-like catalytic domain.

A variety of mechanisms have evolved to maintain REases in inactive configuration to avoid uncontrolled DNA cleavage and couple it to the recognition of specific nucleotide sequence. Orthodox REases, like EcoRI or BamHI, are homodimers that make largely symmetrical interactions with palindromic DNA sequences and contain two distinct sites each responsible for catalyzing cleavage in one DNA strand (1). In orthodox restriction enzymes, structural elements involved in sequence recognition are grafted on the conserved λ-exonuclease-like scaffold that makes a catalytic core (6). Structural analysis indicates that EcoRI amino acid residues involved in specific DNA binding are coupled to the catalytic residues through the intricate network of interactions (7). Therefore, any perturbation in the recognition site (for example, an incorrect base pair) would propagate via the network to the cleavage site and thus prevent DNA cutting at the incorrect site.

Different mechanisms of the activity control are used by type IIS REases. Most type IIS REases are monomers and recognize asymmetric nucleotide sequences. The archetypal type IIS enzyme FokI exhibits a modular architecture and consists of two functional domains: the N-terminal DNA recognition domain and the C-terminal catalytic domain (8). FokI binds DNA as a monomer, with the N-terminal recognition domain making all of the base-specific contacts at the recognition site (8). The catalytic C-terminal domain of FokI exhibits a λ-exonuclease-like fold similar to the orthodox REases (8) and possesses a weak nonspecific nuclease activity (9). Control of nuclease activity in FokI is achieved by two different mechanisms. First, the catalytic domain is sequestered by the recognition domain in a "piggyback" fashion preventing contact with DNA at the cleavage site (8). Second, FokI has only one catalytic site per monomer; therefore, dimerization of two C-terminal domains is required to achieve a double-strand break in DNA (10–12). Association of the catalytic domains of FokI is much more effective when FokI monomers are bound to the separate DNA sites on the same DNA molecule (10). Thus, rearrangement of FokI triggered by specific DNA binding promotes DNA cleavage and limits it to the specific sites.

Yet, another type of mechanism of DNA cleavage control is used by the EcoRII enzyme that belongs to the type IIE subtype of REases. EcoRII requires two copies of the CCWGG recognition sequence for the optimal activity but cleaves only one copy before the first C; the second copy acts as an allosteric activator for the cleavage of the first DNA copy. Structural and biochemical studies demonstrate a modular architecture of EcoRII (13, 14). Proteinase treatment of EcoRII generates the N-terminal allosteric DNA-binding domain and C-terminal domain dimer that cleaves DNA in a site-specific manner (14). Apo-structure of EcoRII suggests (13) that N-terminal allosteric DNA-binding domain sterically blocks DNA access to the catalytic C-terminal domain. Binding of the first DNA copy at the allosteric site triggers enzyme rearrangement and promotes binding and cleavage of the second DNA copy at the C-terminal domain.

BfiI is a type IIS REase that acts at an asymmetric sequence, 5′-ACTGGG-3′, and cuts top and bottom strands at fixed

Conflict of interest statement: No conflicts declared.

Freely available online through the PNAS open access option.

Abbreviations: PLD, phospholipase D; REase, restriction endonuclease.

Data deposition: The atomic coordinates and structure factors have been deposited in the Protein Data Bank, www.pdb.org (PDB ID code 2C1L).

†To whom correspondence may be addressed. E-mail: grazulis@ibt.lt, huber@biochem.mpg.de, or siksnys@ibt.lt.

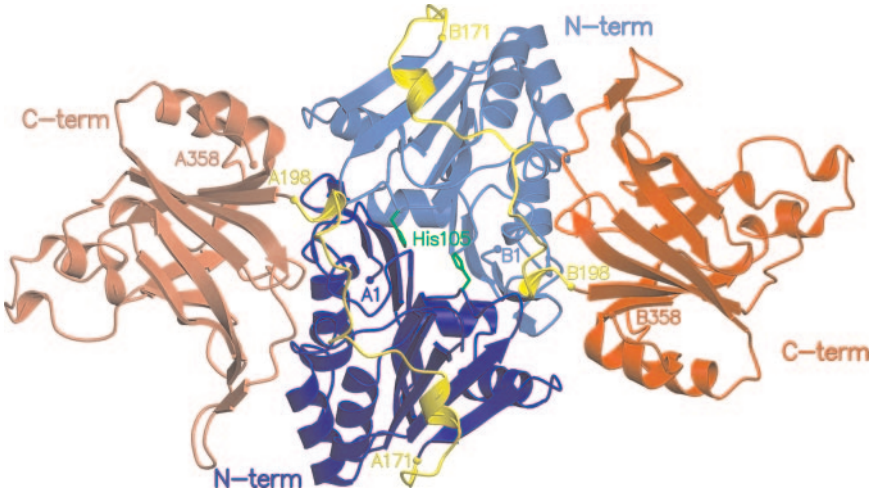

Fig. 1. Crystal structure of BfiI dimer. Two N-terminal domains of each monomer depicted in light and dark blue, respectively, make a dimeric catalytic core flanked by C-terminal DNA-binding domains depicted in light and dark red. The linker connecting the N- and C-terminal domains within the monomer is shown in yellow.

positions downstream of this site (15). In this respect, it is similar to FokI but unique among all of the restriction enzymes found to date by its metal-independence (16). BfiI must therefore hydrolyze phosphodiester bonds by a novel mechanism.

The N-terminal domain of BfiI shows sequence similarity to Nuc, an EDTA-resistant nuclease from the phospholipase D (PLD) superfamily (16, 17). BfiI presumably evolved through the domain fusion of a DNA-recognition element to a nonspecific nuclease akin to Nuc and acquired specificity and function of a restriction enzyme. To gain insight into the architecture of the unique Mg^{2+}-independent restriction enzyme, we have determined the crystal structure of BfiI at 1.9-Å resolution.

Materials and Methods

Protein Crystallization. Wild-type BfiI protein was purified as described in ref. 18. The purified protein was stored at −20°C in a storage buffer containing 50% glycerol, 200 mM KCl, 10 mM Tris·HCl (pH 7.5), 1 mM DTT, and 1 mM EDTA at concentration of ≈3 mg/ml. Immediately before crystallization an aliquot of protein was rebuffered by adding an equal volume of saline buffer (400 mM NaCl/20 mM Tris·HCl, pH 8.5/1 mM EDTA) and concentrated in Centricons (10-kDa cutoff; Millipore) to the final concentrations of ≈3–4 mg/ml. Crystals were prepared by mixing in a 1:1 ratio of the concentrated BfiI solution with the precipitating solution containing 1.2–1.6 M K/Na tartrate and 75 mM Na-MES (pH 6.5). Drops were equilibrated against the reservoir solution that was prepared by adding glycerol to a final concentration of 25% into the precipitating solution. Crystals grew at 19°C in sitting-drop vapor-diffusion crystallization plates.

Data Collection and Structure Determination. Crystals were briefly soaked in reservoir buffer with glycerol concentration increased to 30% and flash-cooled in a nitrogen gas stream (100K). Native data from the BfiI crystals were collected on the European Synchrotron Radiation Facility ID13 synchrotron beamline microdiffractometer (19). A charge-coupled device detector (MAR-Research, Hamburg) allowed the recording of native data to 1.9-Å resolution. Data were processed with the programs MOSFLM (20), SCALA (21), and TRUNCATE (22). For phasing, heavy metal soak diffraction data (see Table 1, which is published as supporting information on the PNAS web site) were collected on the rotating anode source (RU-300) with an image plate detector (Mar345, MAR-Research). Two strong positions of mercury in $HgCl_2$ could be easily identified that allowed for the determination of other derivatives in difference Fourier maps. Phases were calculated to 3.0 Å by using MLPHARE [CCP4 suite (23)], and the MIR (multiple isomorphous replacement) map was solvent-flattened with DM (24). The resulting map clearly showed a β-sheet-containing area, which could be recognized as a catalytic domain of BfiI from the similarity with Nuc nuclease. Phases from the CNS-refined Nuc poly(Ala) chain, combined with the experimental MIR phases in SIGMAA (25), gave a new map where some parts of the C-terminal domain were visible. By using iterative procedure of manual building, most of the C-terminal domain main chain was built. After several iterations of the building cycle at 3.0-Å resolution, no new density appeared, and the model was repositioned for the 1.9-Å synchrotron data set. The model itself, however, did not produce sufficiently good phases to continue with the model building. Therefore, a procedure suggested in the ARP/WARP (26) manual was undertaken. Phases were taken from the MIR data at 3.0 Å (the data had a slightly different cell), merged with the 1.9-Å synchrotron data, and solvent-flattened with DM. The resulting phases were combined with the phases from the partial model that was rigid-body-refined in the new data. The resulting maps, although not traceable with ARP/WARP, showed new details that enabled to complete the model manually to good levels of correspondence with the experimental data (Table 1). Initially, the structure was refined by using the CNS suite, but at the final stages REFMAC (27) gave better R factors and better fit to the maps. However, there were still problems with the refinement of some of our cofactors, because too many bond angles and lengths deviated severely from ideal values if REFMAC was used with default settings. Therefore, at the last stage, the REFMAC bond restraints were made stricter, and then the model was refined with CNS again, allowing just cofactors to change. This yielded a model almost without geometry violations and good R factors. In the refined structure, all protein residues except one fall into the most favored and additionally allowed Ramachandran plot regions (28). Figures of the molecules were produced by using the programs MOLSCRIPT (29), RASTER3D (30), and MOLMOL (31).

Results

Overall Structure: Domain Architecture of BfiI. Electron densities calculated at 1.9-Å resolution (see Fig. 5, which is published as supporting information on the PNAS web site) show all of the protein chain except for a loop between residues 246 and 249 in the chain B (see Fig. 6, which is published as supporting information on the PNAS web site, for the topological diagram of BfiI). The crystal structure of the BfiI reveals two chains in the asymmetric unit (Fig. 1). Each chain is folded into two distinct globular domains (Fig. 1). Both domains are connected by a

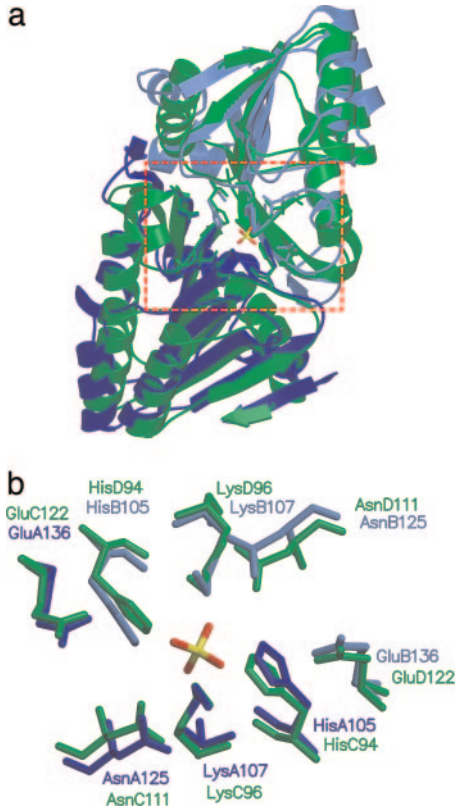

Fig. 2. Comparison of BfiI with EDTA-resistant nonspecific Nuc nuclease from *S. typhimurium*. (*a*) Structural superposition of the N-terminal domain dimer of BfiI (light and dark blue) and Nuc nuclease (green). The active-site region of Nuc nuclease is boxed in red. (*b*) Close-up view of the active-site residues of Nuc nuclease (green) and their structural equivalents in BfiI (light and dark blue) shown in the same orientation as in *a*. The tungstate molecule coordinated at the putative scissile DNA phosphate-binding site in Nuc is shown in stick representation colored by atom type. Amino acid residues from both subunits of Nuc and BfiI contribute to a single active site located in the intersubunit cleft.

stretch of amino acid residues (171–198) mostly in extended conformation, which is flanked by short 3_{10}-helices on both ends. The N-terminal domains form a dimer (Fig. 1), which presumably represents the structure of the functionally active BfiI dimer in solution (18). C-terminal domains within this dimer are situated on the opposite sides of the N-terminal domain core and make no contacts to each other. The overall shape of the BfiI molecule resembles a two-axial ellipsoid with a short axis of ≈55 Å and a long axis of 100 Å, respectively. All four domains are positioned along the long ellipsoid axis in the order C-NN-C.

The N-Terminal Domain of BfiI: Similarities to Nuc Nuclease. The N-terminal domain of BfiI extends from Met-1 to Met-170. It is arranged as an eight-stranded β-sheet flanked by three α-helices on one side and two α-helices on the other side (Figs. 1 and 6). The N-terminal domains of BfiI are folded into an α/β-globule through dimerization of two β-sheets of individual chains. A DALI (32) database search for similar three-dimensional structures revealed a high similarity (Z = 15.4) to the *Salmonella typhimurium* Nuc nuclease (17) [Protein Data Bank (PDB) entry 1BYR] that belongs to the PLD superfamily (Fig. 2*a*). Human tyrosyl-DNA phosphodiesterase Tdp1 (33) (PDB entry 1JY1) and PLD (34) (PDB entry 1F0I) from *Streptomyces*, both members of the PLD superfamily, also show a high degree of structural similarity to the N-terminal domain of BfiI (DALI Z scores of 8.9 and 9.6, respectively). Structural similarities confirm earlier biochemical and mutational studies indicating that BfiI is a member of PLD family (16, 18).

Upon structural superposition with TOP3D (35), amino acid residues His-105, Lys-107, Asn-125, and Glu-136 of BfiI that are important for the catalytic activity (18) closely superimpose with His-94, Lys-96, Asn-111, and Glu-122 residues at the active site of Nuc (17, 36) (Fig. 2*b*). These residues of BfiI and Nuc display the same side-chain rotamers in both structures and can be superimposed with an rms deviation of 1.4 Å. The conservation of the active-site residues between Nuc and the N-terminal domain of BfiI (Fig. 2*b*) provides important insights into the mechanism of catalysis by BfiI. In the Nuc dimer, the conserved His-94, Lys-96, and Glu-122 residues from both subunits contribute to the single active site located in the cleft between the two monomers (Fig. 2*b*). It has been suggested that Nuc catalysis proceeds with the formation of a phosphoenzyme intermediate that is subsequently hydrolyzed to form the final product (17, 36). The conserved active-site His-94 residue in one of the monomers has been directly implicated as a nucleophile in the reaction leading to the covalent intermediate, while the symmetry-related His from another subunit acts as a general acid protonating the leaving group (36). Conservation of the key catalytic residues between Nuc and BfiI implies similar chemistry of phosphodiester bond cleavage; however, the formation of the covalent intermediate for BfiI has yet to be demonstrated.

The N-terminal domain of BfiI, similarly to the human tyrosyl-DNA phosphodiesterase Tdp1, lacks the conserved aspartate residue of HKD motif characteristic to Nuc and *Streptomyces* PLD (37). According to the crystal structures, the latter residue is not a part of the active site of Nuc (17) and *Streptomyces* PLD (34), and it is thought to be important for the stabilization of the tertiary structure. Because of this distinction, human tyrosyl-DNA phosphodiesterase Tdp1 and its orthologs were assigned into a separate subclass within the PLD superfamily (37). BfiI is suggested to be a member of this subfamily.

The C-Terminal Domain of BfiI: Similarities to Mg^{2+}-Dependent REase and Plant Transcription Factors. The C-terminal domain of BfiI extends from Val-199 to Phe-358. It is comprised of two β-sheets (Figs. 1 and 3*a*) that are interconnected through β13 and β14 strands, shared by both sheets (Fig. 6). The two β-sheets are sandwiched together into a barrel-like structure, composed of eight β-strands (β10, β11, β13–β17, and β19). The "barrel," however, is not closed because strands β11 and β19 are not hydrogen-bonded. Two additional short β-strands (β12 and β18) and three α-helices are located outside the pseudobarrel.

A DALI database search revealed that the C-terminal domain of BfiI is significantly similar (Z = 8.8) to the N-terminal domain of Mg^{2+}-dependent REase EcoRII that belongs to the type IIE subtype. Another significant similarity (Z = 7.1) is to the B3 DNA-binding domain of *Arabidopsis* cold-responsive transcription factor RAV1 (38) (PDB entry 1WID), specific for the CACCTG sequence (39). A structural superposition of the C-terminal domain of BfiI, the N-terminal domain of EcoRII REase, and the RAV1 transcription factor of *Arabidopsis* (Fig. 3*a*) clearly shows that all three domains represent the same fold.

The structures of BfiI, EcoRII (13), and the B3-domain of RAV1 transcription factor of *Arabidopsis* (38) were solved in a DNA-free form. Structural similarities between the C-terminal domain of BfiI, the N-terminal domain of EcoRII, and the B3-domain of RAV1 (Fig. 3*a*), however, provide some clues regarding the putative DNA-binding surface. Topologically similar concave clefts laid by the positively charged residues and large enough to accommodate a DNA molecule could be identified in all domains (see Fig. 7, which is published as supporting information on the PNAS web site). Cross-linking and mutational studies of EcoRII demonstrated the importance of His-36, Tyr-41, Lys-92, Arg-94, Glu-96, Lys-97, and Arg-98

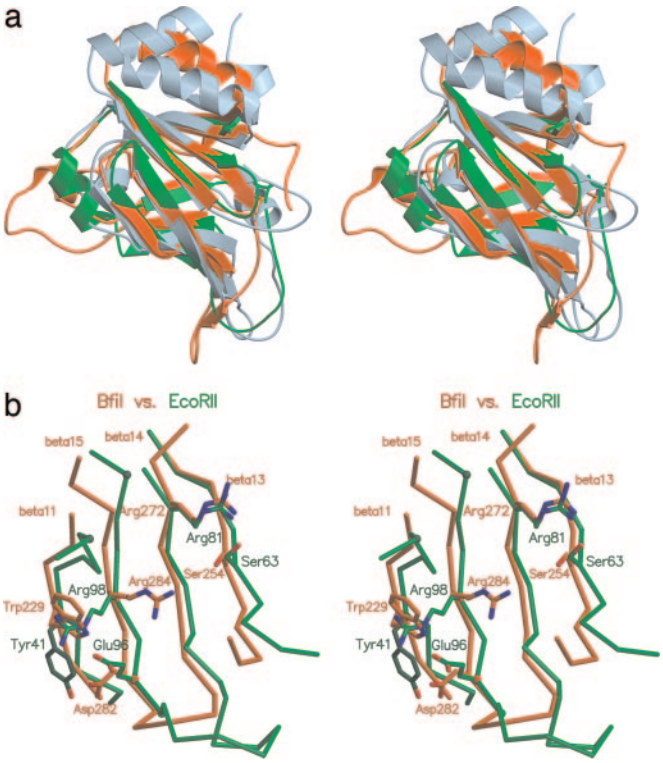

Fig. 3. Structural comparison of the C-terminal DNA-binding domain of the metal-independent REase BfiI, the N-terminal effector DNA-binding domain of type IIE restriction enzyme EcoRII, and the B3 DNA-binding domain of plant transcription factor RAV1. (*a*) Structural overlay of DNA-binding domains of BfiI (red), EcoRII (green), and RAV1-B3 (blue). (*b*) Stereoview of the backbone atom superposition in the putative DNA-binding clefts of BfiI (red) and EcoRII (green). The EcoRII residues important for DNA binding are shown as sticks colored by atom type, with carbon atoms in green. Structurally equivalent BfiI residues are shown as sticks with carbon atoms in red.

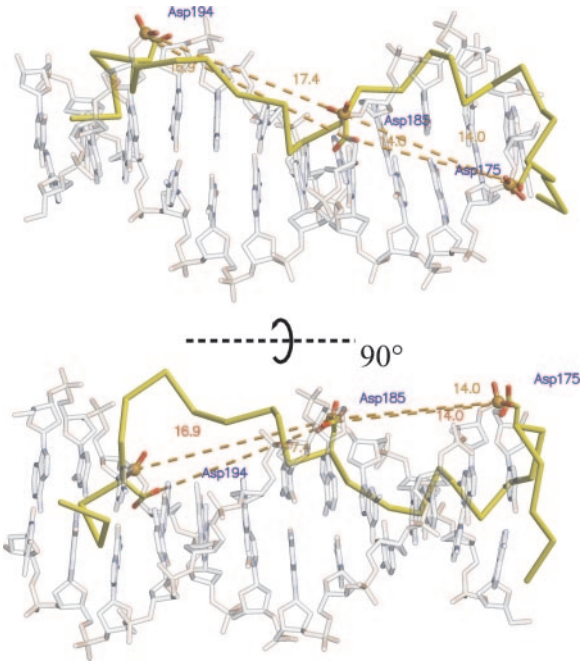

Fig. 4. DNA backbone mimic by the interdomain linker of BfiI. The linker region is shown as a C_α trace; Asp residues are labeled and shown in stick representation. Distances between C_γ atoms of Asp residues are shown as yellow dashed lines. The B-DNA molecule (Nucleic Acid Database ID bd0001) is shown in gray. DNA backbone phosphate atoms equivalent to Asp C_γ atoms are shown as yellow spheres. Superposition of BfiI linker peptide and DNA was obtained by superimposing C_γ atoms of linker aspartates (Asp-175, -185, and -194) onto the DNA's closest possible phosphate and C_α of the same residues onto DNA O_4' atoms of the corresponding nucleotides.

residues located in the cleft for the effector DNA binding (40, 41). NMR-titration experiments revealed a similar protein–DNA interface in RAV1-B3 (38). The equivalent cleft in BfiI is suggested to contribute to specific DNA binding. C_α atoms of BfiI residues Trp-229, Asp-282, and Arg-284 (Fig. 3*b*) spatially correspond to EcoRII residues Tyr-41, Glu-96, and Arg-98, which are important for DNA binding (41). Their side chain rotamers differ but may change in the presence of DNA. In addition, Arg-272 and Ser-254 residues of BfiI coincide with Arg-81 and Ser-63 residues of EcoRII. The functional importance of these residues so far has not yet been tested. The conservation of some residues in the DNA-binding clefts of BfiI and EcoRII is intriguing in view of the different recognition sequences (ACTGGG in the case of BfiI and CCWGG for EcoRII).

Interdomain Interface. N- and C-terminal domains in a BfiI monomer make an extensive set of hydrophobic contacts between the "inner" faces of the β-sheet. Approximately 1,700 Å^2 are buried at the interdomain interface in BfiI monomer. Contacts of the C-terminal domain to the N-terminal domain of the neighboring subunit (i.e., C terminus of chain A with the N terminus of the chain B) contribute an additional 500 Å^2 to the interdomain interface. Thus, the two domains have a relatively large interdomain interface of $\approx$2,200 Å^2, characteristic of specific protein–protein interactions (42). In comparison, the main dimer interface of the BfiI formed by the N-terminal domains buries 3,500 Å^2 (Fig. 1).

The C-terminal DNA-binding domain of BfiI and the N-terminal effector DNA-binding domain of EcoRII are similar to the B3-like DNA-binding domain of plant-specific transcription factors (Fig. 3*a*). Hence, the transcription factor-like DNA-binding domain has been used not only to confer DNA specificity to a PLD family nuclease, to give the metal-free BfiI enzyme as shown here, but also to create allosteric site(s) in an orthodox PD . . . EXK family enzyme, to generate the metal-dependent type IIE restriction enzyme EcoRII. Although the C-terminal DNA-binding domain of BfiI is structurally similar to the N-terminal effector DNA-binding domain of EcoRII, they employ different interfaces to interact with the corresponding catalytic domains (see Fig. 8, which is published as supporting information on the PNAS web site). In BfiI, the DNA-binding domain makes contacts predominantly with the catalytic N-terminal domain of the same chain, making hydrogen bonds and hydrophobic contacts through residues coming from the edge of the first barrel-forming β-sheet (strands β13–β15 and extended region connecting strands β11 and β12). In contrast, in EcoRII the effector DNA-binding N-terminal domain contacts the catalytic domain through the residues located on α-helices and their flanking loop regions (13). Thus, DNA-binding domains of BfiI and EcoRII possess a similar DNA-binding cleft but are oriented differently with respect to their catalytic cores. Moreover, whereas the DNA-binding domains of BfiI are spatially separated, the N-terminal domains of EcoRII contact each other and contribute to the dimer interface.

Interdomain Peptide Linker: Possible Role in Activity Control. The linker connecting the N- and C-terminal domains of the BfiI contains a stretch of 28 amino acid residues (171–198) that predominantly has an extended conformation (Fig. 4). The

linker runs across the putative DNA-binding surface at the N-terminal domain of BfiI close to the entrance to the active site buried at the interface between the two domains (Fig. 1). It contains a number of negatively charged Asp and Glu residues. Interestingly, three Asp residues (Asp-175, -185, and -194) are spaced at distances very close to those between the phosphates of a B-DNA backbone (Fig. 4). One might speculate that the interdomain linker in BfiI mimics the DNA backbone similarly to the Ocr antirestriction protein (43) and acts as an intramolecular inhibitor that represses nucleolytic activity of the catalytic N-terminal domain by occluding the DNA-binding surface.

Discussion

The crystal structure of BfiI (Fig. 1) reveals a novel domain architecture consistent with previously reported limited proteolysis (44) data, where the N terminus is shown to be an unspecific nuclease and the C terminus is a DNA-binding domain. The crystal structure of BfiI demonstrates how nature can reconfigure protein domains for new functions. In BfiI, a DNA-recognition element is fused to a nonspecific nuclease core family to generate a REase. In the asymmetric unit, two N-terminal domains of BfiI are arranged into a dimer structurally similar to the nonspecific EDTA-resistant Nuc nuclease (Fig. 2) that belongs to the PLD superfamily. Structural similarities between BfiI, Nuc nuclease (17), tyrosyl-DNA phosphodiesterase Tdp1 (33), and PLD (34) provide a direct link between BfiI and the PLD superfamily, a diverse group of proteins that includes phospholipases, phospholipid synthases, bacterial toxins, pox virus envelope proteins, phosphodiesterases, and bacterial nucleases (45). PLD-family enzymes exhibit a conserved catalytic core and share a common catalytic mechanism; however, these enzymes encompass a very broad range of substrate specificities (45). Different enzymes in the PLD family may therefore have evolved through the fusion of a common catalytic core to separate domains for substrate recognition.

The C-terminal DNA-binding domain of BfiI (Fig. 3*a*) is structurally similar to the N-terminal DNA-binding domain of Mg^{2+}-dependent REase EcoRII (13). This finding suggests that different subtypes and lineages of REases might have evolved through the recombination of conserved structural blocks that became fused to different catalytic cores.

Strikingly, DNA-binding domains of EcoRII/BfiI and B3 DNA-binding domain of *Arabidopsis* cold-responsive transcription factor RAV1 (38) share a similar structural fold (Fig. 3*a*). The B3-like DNA-binding domain was thought to be plant-specific and belongs to the family that currently includes ≈300 proteins (InterPro IPR 003340) involved in the auxin-regulated and abscisic acid-regulated transcription (46). Identification of structural and functional homologues of the "plant-specific" B3 DNA-binding domain in the bacteria kingdom provokes speculations on the possible evolutionary relationships.

A PSI-BLAST search of the protein sequence database by using BfiI sequence as a query reveals significant similarities to the hypothetical protein MBNC03000766 of *Mesorhizobium* sp. BNC1 strain (see Fig. 9, which is published as supporting information on the PNAS web site). The degree of sequence similarity (60% of identical and 76% of similar amino acids) indicates that the unknown protein MBNC03000766 of *Mesorhizobium* sp. BNC1 strain is likely to be a restriction enzyme similar to BfiI. Moreover, typically for type IIS restriction modification system gene organization two ORFs possessing similarities to the DNA-methyltransferases are found in the vicinity of the gene of putative *Mesorhizobium* sp. BNC1 endonuclease (data not shown). Interestingly, the *Mesorhizobium* sp. BNC1 strain subjected for the genome sequencing has been isolated from an enrichment of industrial sewage receiving EDTA-containing wastewater effluents added to surface soil. This strain is able to use EDTA as a sole source of carbon and nitrogen, and thrives in an EDTA-rich environment (47). In such a metal-ion hostile environment, the presence of EDTA-resistant REase in bacteria might be an advantage.

Both the N- and C-terminal domains of BfiI (Fig. 1) represent independent structural and functional modules. The isolated DNA-binding domain binds specifically to the 5′-ACTGGG sequence characteristic for BfiI, whereas the N-terminal domain possesses a nonspecific nuclease activity (44). Mixing of the isolated N- and C-terminal domains, however, does not reconstitute the ability of BfiI to cleave phosphodiester bonds at specific sites (M. Zaremba and V.S., unpublished data). Thus, to function as a restriction enzyme, BfiI had to elaborate a nuclease activity control mechanism to limit double-strand breaks at the specific recognition sequence. The crystal structure of BfiI suggests how interdomain communications can lead to novel protein functions, not possessed by either domain alone.

BfiI, like many orthodox Mg^{2+}-dependent REases, is a dimer in solution (18). In contrast to the dimeric enzymes that recognize a single copy of their DNA, the dimeric form of BfiI binds two copies of its recognition sequence (18). Yet, when bound to two copies of its recognition site, the BfiI dimer cleaves only one phosphodiester bond at a time (48). The crystal structure reveals that BfiI, like Nuc from *S. typhimurium*, has a single active site located at the interface between the N-terminal domains (Fig. 2 *a* and *b*). Similarly to Nuc, an isolated N-terminal domain of BfiI degrades DNA containing or lacking BfiI recognition sequence by introducing random cuts (44). Structural superposition between BfiI and Nuc reveals that in the wild-type BfiI the linker region interconnecting N- and C-terminal domains crosses the putative DNA-binding surface of the catalytic domain (Fig. 1) and sterically interferes with DNA binding. Distribution of negatively charged residues in the interdomain linker suggests that it might mimic the DNA backbone (Fig. 4) and autoinhibit the DNA cleavage. The BfiI conformation seen in the crystal may therefore represent a latent form. The active site of BfiI, however, remains available for small artificial substrates like bis-*p*-nitrophenyl phosphate, which is hydrolyzed by BfiI (16). Thus, the negatively charged linker in BfiI does not disrupt the active site but rather creates a steric block for DNA binding.

To cleave DNA, the binding surface at the N-terminal domain must become available for DNA binding. Proteolytic cleavage of BfiI opens an access for DNA binding at the active site located at the catalytic domain, but phosphodiester bond hydrolysis then occurs at random rather than at specific sites (44). Thus, to focus cleavage at particular DNA sites, the opening of the catalytic domain in the wild-type BfiI has to be coupled to the specific DNA binding (see Fig. 10, which is published as supporting information on the PNAS web site). We propose that specific DNA binding to the C-terminal domain of BfiI may trigger a conformational rearrangement that leads to repositioning of the linker and unveils a surface for DNA binding at the catalytic N-terminal domain (Fig. 10). Such a cognate DNA-binding-induced conformational switch juxtaposes the catalytic domain in a proper configuration to enable BfiI to cleave a phosphodiester bond (48). The single active site in the dimeric catalytic domain then acts sequentially on the four target phosphodiester bonds. It has yet to be determined how the four target bonds, two from each recognition site, are placed in turn into the single active site of the enzyme.

We thank V. Stonyte for help with purification of the BfiI protein and S. Halford of the University of Bristol (Bristol, UK) and M. Zaremba, G. Sasnauskas, and C. Venclovas of the Institute of Biotechnology (Vilnius) for discussions and critical reading of the manuscript. Data sets were collected on the ID13 beamline of the European Synchrotron Radiation Facility (Grenoble), the European Molecular Biology Laboratory X13 beamline of the Deutsches Elektronen Synchrotron (Hamburg), and the International Institute of Molecular and Cell Biology (Warsaw). Measurements at the European Molecular Biology Labora-

tory outstation were supported by the European Community Access to Research Infrastructure Action of the Improving Human Potential Program. V.S. is a recipient of Lithuanian State Fellowship. The work at the Institute of Biotechnology (Vilnius) was supported in part by the Howard Hughes Medical Institute, the Wellcome Trust, the Max Planck Society, and the Lithuania State Science and Studies Foundation.

1. Pingoud, A., Fuxreiter, M., Pingoud, V. & Wende, W. (2005) *Cell Mol. Life Sci.* **62,** 685–707.
2. Kovall, R.A. & Matthews, B.W. (1998) *Proc. Natl. Acad. Sci. USA* **95,** 7893–7897.
3. Ban, C. & Yang, W. (1998) *EMBO J.* **17,** 1526–1534.
4. Lilley, D. M. & White, M. F. (2000) *Proc. Natl. Acad. Sci. USA* **97,** 9351–9353.
5. Aravind, L., Makarova, K. S. & Koonin, E. V. (2000) *Nucleic Acids Res.* **28,** 3417–3432.
6. Buijnicki, J. M. (2004) in *Restriction Endonucleases*, ed. Pingoud, A. (Springer, Berlin), pp. 63–93.
7. Kurpiewski, M.R., Engler, L. E., Wozniak, L. A., Kobylanska, A., Koziolkiewicz, M., Stec, W. J. & Jen-Jacobson, L. (2004) *Structure* **12,** 1775–1788.
8. Wah, D. A., Hirsch, J. A., Dorner, L. F., Schildkraut, I. & Aggarwal, A. K. (1997) *Nature* **388,** 97–100.
9. Li, L., Wu, L. P. & Chandrasegaran, S. (1992) *Proc. Natl. Acad. Sci. USA* **89,** 4275–4279.
10. Bath, A. J., Milsom, S. E., Gormley, N. A. & Halford, S. E. (2002) *J. Biol. Chem.* **277,** 4024–4033.
11. Wah, D. A., Bitinaite, J., Schildkraut, I. & Aggarwal, A. K. (1998) *Proc. Natl. Acad. Sci. USA* **95,** 10564–10569.
12. Bitinaite, J., Wah, D. A., Aggarwal, A. K. & Schildkraut, I. (1998) *Proc. Natl. Acad. Sci. USA* **95,** 10570–10575.
13. Zhou, E. X., Wang, Y., Reuter, M., Mücke, M., Krüger, D., Meehan, E. J. & Chen, L. (2004) *J. Mol. Biol.* **335,** 307–319.
14. Mucke, M., Grelle, G., Behlke, J., Kraft, R., Kruger, D. H. & Reuter, M. (2002) *EMBO J.* **21,** 5262–5268.
15. Vitkute, J., Maneliene, Z., Petrusyte, M. & Janulaitis, A. (1998) *Nucleic Acids Res.* **26,** 3348.
16. Sapranauskas, R., Sasnauskas, G., Lagunavicius, A., Vilkaitis, G., Lubys, A. & Siksnys, V. (2000) *J. Biol. Chem.* **275,** 30878–30885.
17. Stuckey, J. A. & Dixon, J. E. (1999) *Nat. Struct. Biol.* **6,** 278–284.
18. Lagunavicius, A., Sasnauskas, G., Halford, S. E. & Siksnys, V. (2003) *J. Mol. Biol.* **326,** 1051–1064.
19. Cusack, S., Belrhali, H., Bram, A., Burghammer, M., Perrakis, A. & Riekel, C. (1998) *Nat. Struct. Biol.* **5,** Suppl., 634–637.
20. Leslie, A. G. W. (2003) *MOSFLM 6.2.3 User Guide* (MRC Lab. of Mol. Biol., Cambridge, U.K.).
21. Evans, P. R. (1997) *Joint CCP4 and ESF-EACBM Newsletter* **33,** 22–24.
22. French, G. S. & Wilson, K. S. (1978) *Acta Crystallogr. A* **34,** 517–525.
23. Collaborative Computational Project Number 4 (1994) *Acta Crystallogr. D* **50,** 760–763.
24. Cowtan, K. (1994) *Joint CCP4 and ESF-EACBM Newsletter on Protein Crystallography* **31,** 34–38.
25. Read, R. J. (1986) *Acta Crystallogr. A* **42**, 140–149.
26. Morris, R. J., Perrakis, A. & Lamzin, V. S. (2002) *Acta Crystallogr. D* **58**, 968–975.
27. Murshudov, G. N., Vagin, A. A. & Dodson, E. J. (1997) *Acta Crystallogr. D* **53,** 240–255.
28. Laskowski, R. A., MacArthur, M. W., Moss, D. S. & Thornton, J. M. (1993) *J. Appl. Crystallogr.* **26,** 283–291.
29. Kraulis, P. J. (1991) *J. Appl. Crystallogr.* **24,** 946–950.
30. Merritt, E. A. & Bacon, D. J. (1997) *Methods Enzymol.* **277,** 505–524.
31. Koradi, R., Billeter, M. & Wüthrich, K. (1996) *J. Mol. Graphics* **14,** 51–55.
32. Holm, L. & Sander, C. (1998) *Proteins* **33,** 88–96.
33. Davies, D. R., Interthal, H., Champoux, J. J. & Hol, W. G. J. (2002) *Structure* **10,** 237–248.
34. Leiros, I., Secundo, F., Zambonelli, C., Servi, S. & Hough, E. (2000) *Structure* **8,** 655–667.
35. Lu, G. (2000) *J. Appl. Crystallogr.* **33,** 176–183.
36. Gottlin, E. B., Rudolph, A. E., Zhao, Y., Matthews, H. R. & Dixon, J. E. (1998) *Proc. Natl. Acad. Sci. USA* **95,** 9202–9207.
37. Interthal, H., Pouliot, J. J. & Champoux, J. J. (2001) *Proc. Natl. Acad. Sci. USA* **98,** 12009–12014.
38. Yamasaki, K., Kigawa, T., Inoue, M., Tateno, M., Yamasaki, T., Yabuki, T., Aoki, M., Seki, E., Matsuda, T., Tomo, Y., *et al.* (2004) *Plant Cell* **16,** 3448–3459.
39. Kagaya, Y., Ohmiya, K. & Hattori, T. (1999) *Nucleic Acids Res.* **27,** 470–478.
40. Mücke, M., Pingoud, V., Grelle, G., Kraft, R., Krüger, D. H. & Reuter, M. (2002) *J. Biol. Chem.* **277,** 14288–14293.
41. Reuter, M., Schneider-Mergener, J., Kupper, D., Meisel, A., Mackeldanz, P., Krüger, D. H. & Schroeder, C. (1999) *J. Biol. Chem.* **274,** 5213–5221.
42. Janin, J. (1997) *Nat. Struct. Biol.* **4,** 973–974.
43. Walkinshaw, M. D., Taylor, P., Sturrock, S. S., Atanasiu, C., Berge, T., Henderson, R. M., Edwardson, J. M. & Dryden, D. T. F. (2002) *Mol. Cell* **9,** 187–194.
44. Zaremba, M., Urbanke, C., Halford, S. E. & Siksnys, V. (2004) *J. Mol. Biol.* **336,** 81–92.
45. Ponting, C. P. & Kerr, I. D. (1996) *Protein Sci.* **5,** 914–922.
46. Ulmasov, T., Hagen, G. & Guilfoyle, T. J. (1997) *Science* **276,** 1865–1868.
47. Bohuslavek, J., Payne, J. W., Liu, Y., Bolton, H. J. & Xun, L. (2001) *Appl. Environ. Microbiol.* **67,** 688–695.
48. Sasnauskas, G., Halford, S. E. & Siksnys, V. (2003) *Proc. Natl. Acad. Sci. USA* **100,** 6410–6415.

Table 1. Data collection and refinement statistics

Data collection statistics:							
Dataset:	**L28B2 (native)**	**L28C6 $HgCl_2$**	**L28D2 K_2PtCl_4**	**L88A4 $(NH_4)_2WS_4$**	**L88C1 K_2OsO_4**	**L88A2 EtOHg**	**L88B3_2 Ta_6Br_{14}**
Temperature				RT (290K)			
Spacegroup				I4			
a=b=, Å c=, Å	140.7 97.4	140.9 97.8	140.8 97.8	140.2 97.3	140.6 98.7	141.0 96.8	140.9 96.4
Resolution, Å (final shell)	48.8 – 3.5 (3.7 – 3.5)	48.8 – 3.4 (3.6 – 3.4)	40.5 – 3.5 (3.7 – 3.5)	42.3 – 2.5 (2.7 – 2.5)	40.5 – 3.0 (3.16 – 3.0)	28.7 – 3.4 (3.58 – 3.4)	48.2 – 2.8 (2.97 – 2.8)
Reflections unique (total)	12100 (45984)	13281 (49702)	12002 (35629)	30889 (114411)	18290 (36609)	12785 (30504)	22711 (85677)
Completeness (%) overall (final shell)	100.0 (100.0)	100.0 (100.0)	98.9 (99.8)	99.0 (93.7)	95.2 (97.6)	97.4 (98.8)	99.2 (95.3)
I/σ_I overall (final shell)	2.8 (1.3)	4.1 (2.2)	3.3 (1.3)	7.9 (2.4)	2.9 (0.6)	4.5 (2.1)	2.6 (1.5)
[a]R_{merge} overall	21 %	15.7 %	18.3 %	7.7 %	19.4 %	13.7 %	15.4 %
Number of heavy atom sites	-	4	10	4	3	12	1×6
[b]Phasing power (centric/acentric)	-	0.92/1.2	0.79/1.2	0.56/0.89	0.81/1.03	1.07/1.45	1.05/1.15
[c]FOM (MIR)	0.58	-	-	-	-	-	-

Refinement statistics:			
Dataset:	**L18B1 (native)**		
Temperature	90K	Number of atoms	6445
Spacegroup	I4	Number of solvent molecules	468
a=b=, Å c=, Å	138.9 94.1	Number of bounded buffer molecule atoms	66
Resolution, Å (final shell)	28.0 – 1.9 (2.0 – 1.9)	Test set size	10% random
Reflections unique (total)	70374 (268268)	[d]R_{cryst} (R_{free})	0.187 (0.218)
Completeness (%) overall (final shell)	99.9 (100.0)	RMS bonds/angles	0.017 Å/1.6°
I/σ_I overall (final shell)	10.4 (2.7)	Average B-factors (Å^2)	
		main chain	25.2
		side chains	26.6
		solvent	35.5
		cofactors	56.7
[a]R_{merge} overall	4.9 %		

[a] $R_{merge} = \Sigma_{\boldsymbol{h}} \Sigma_{i=1}^{n_{\boldsymbol{h}}} \left| \langle I_{\boldsymbol{h}} \rangle - I_{\boldsymbol{h}i} \right| / \Sigma_{\boldsymbol{h}} \Sigma_{i=1}^{n_{\boldsymbol{h}}} \left| I_{\boldsymbol{h}i} \right|$, where $I_{\boldsymbol{h}i}$ is an intensity value of i-th measurement of reflection $\boldsymbol{h}$, $\boldsymbol{h} = (h, k, l)$, sum $\Sigma_{\boldsymbol{h}}$ runs over all measured reflections, and $\langle I_{\boldsymbol{h}} \rangle$ is an average measured intensity of the reflection $\boldsymbol{h}$. Number $n_{\boldsymbol{h}}$

is a number of measurements of reflection ***h***. Data were processed with MOSFLM [Leslie 2003] and further processed SCALA [Evans 1997] and TRUNCATE [French 1978] from CCP4 [CCP4 1994] package.

[b] Phasing power = $\langle |F_{\boldsymbol{h}}^{obs}| \rangle / r.m.s.d.\, \varepsilon$, where ε is lack of closure.

[c] FOM – Figure of merit

[d] $R_{crys,\,free} = \Sigma_{\boldsymbol{h}} |F_{\boldsymbol{h}}^{obs} - F_{\boldsymbol{h}}^{calc}| / \Sigma_{\boldsymbol{h}} |F_{\boldsymbol{h}}^{obs}|$, where $F_{\boldsymbol{h}}^{obs}$ and $F_{\boldsymbol{h}}^{calc}$ are observed and calculated structure factors, respectively.

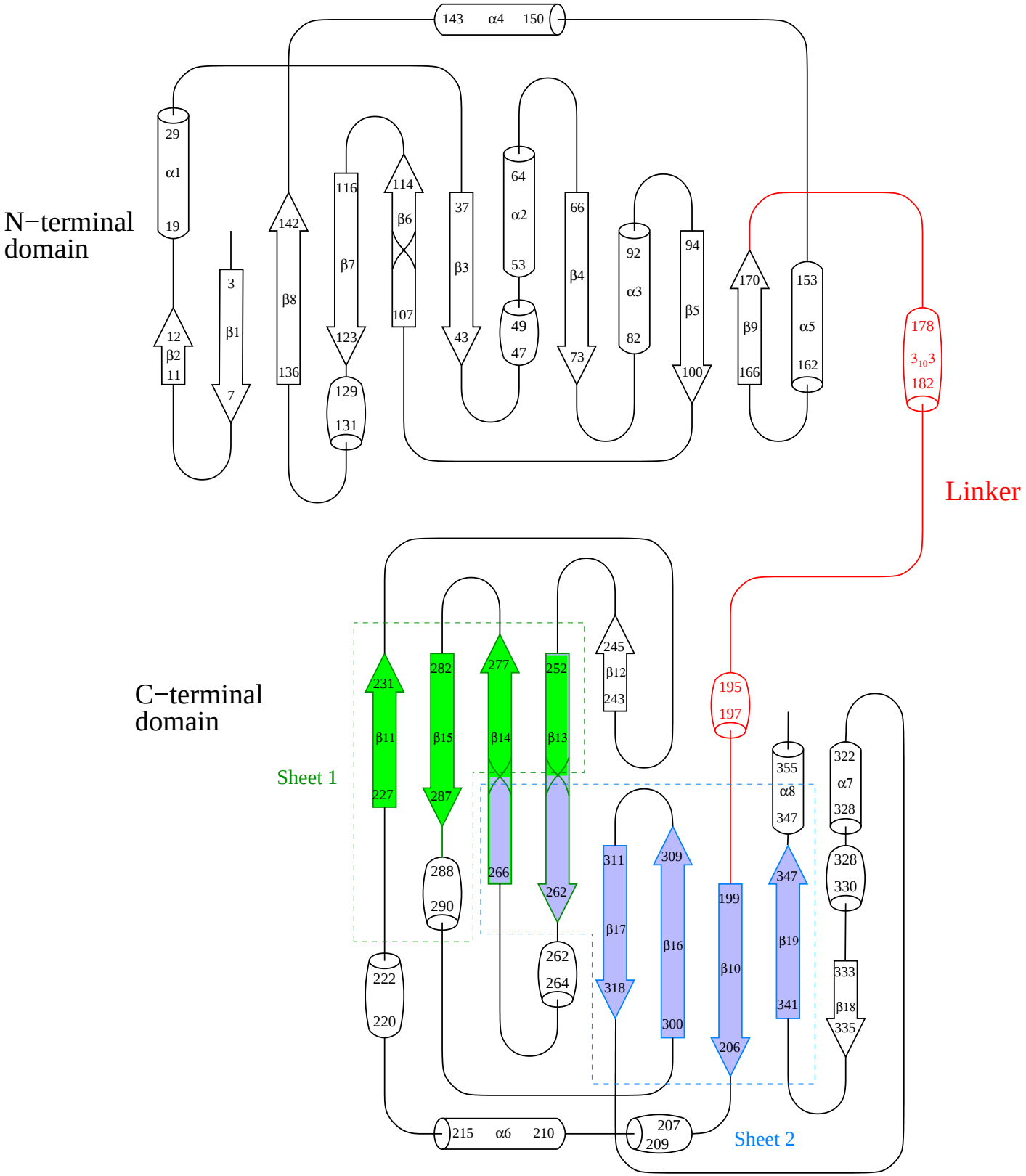
N−terminal domain
C−terminal domain
Linker
Sheet 1
Sheet 2
143 α4 150
29 α1 19
3 β1 7
12 β2 11
142 β8 136
116 β7 123
129 131
114 β6 107
37 β3 43
64 α2 53
49 47
66 β4 73
92 α3 82
94 β5 100
170 β9 166
153 α5 162
178 3₁₀3 182
195 197
231 β11 227
282 β15 287
277 β14 266
252 β13 262
245 β12 243
288 290
262 264
222 220
311 β17 318
309 β16 300
199 β10 206
355 α8 347
347 β19 341
322 α7 328
328 330
333 β18 335
215 α6 210
207 209

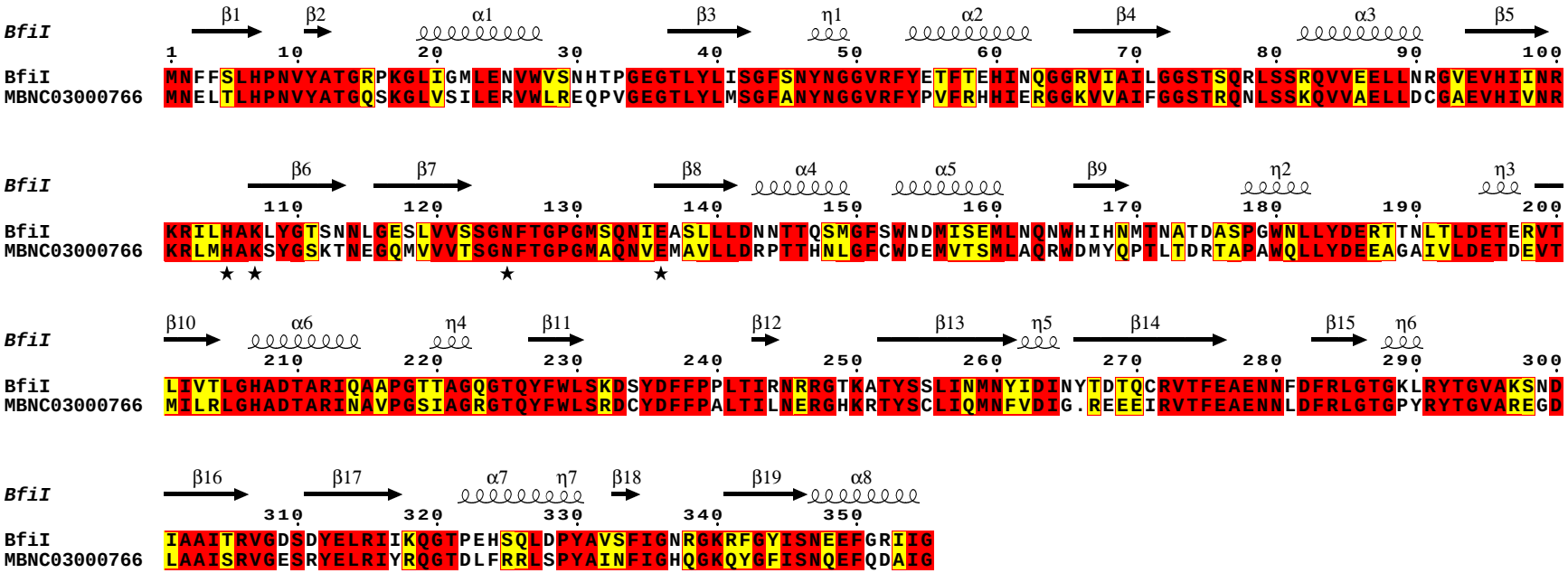
BfiI
β1 β2 α1 β3 η1 α2 β4 α3 β5
1 10 20 30 40 50 60 70 80 90 100
BfiI MNFFSLHPNVYATGRPKGLIGMLENVWVSNHTPGEGTLYLISGFSNYNGGVRFYETFTEHINQGGRVIAILGGSTSQRLSSRQVVEELLNRGVEVHIINR
MBNC03000766 MNELTLHPNVYATGQSKGLVSILERVWLREQPVGEGTLYLMSGFANYNGGVRFYPVFRHHIERGGKVVAIFGGSTRQNLSSKQVVAELLDCGAEVHIVNR
BfiI
β6 β7 β8 α4 α5 β9 η2 η3
110 120 130 140 150 160 170 180 190 200
BfiI KRILHAKLYGTSNNLGESLVVSSGNFTGPGMSQNIEASLLLDNNTTQSMGFSWNDMISEMLNQNWHIHNMTNATDASPGWNLLYDERTTNLTLDETERVT
MBNC03000766 KRLMHAKSYGSKTNEGQMVVVTSGNFTGPGMAQNVEMAVLLDRPTTHNLGFCWDEMVTSMLAQRWDMYQPTLTDRTAPAWQLLYDEEAGAIVLDETDEVT
★ ★ ★ ★
BfiI
β10 α6 η4 β11 β12 β13 η5 β14 β15 η6
210 220 230 240 250 260 270 280 290 300
BfiI LIVTLGHADTARIQAAPGTTAGQGTQYFWLSKDSYDFFPPLTIRNRRGTKATYSSLINMNYIDINYTDTQCRVTFEAENNFDFRLGTGKLRYTGVAKSND
MBNC03000766 MILRLGHADTARINAVPGSIAGRGTQYFWLSRDCYDFFPALTILNERGHKRTYSCLIQMNFVDIG.REEEIRVTFEAENNLDFRLGTGPYRYTGVAREGD
BfiI
β16 β17 α7 η7 β18 β19 α8
310 320 330 340 350
BfiI IAAITRVGDSDYELRIIKQGTPEHSQLDPYAVSFIGNRGKRFGYISNEEFGRIIG
MBNC03000766 LAAISRVGESRYELRIYRQGTDLFRRLSPYAINFIGHQGKQYGFISNQEFQDAIG